Urban Heat Island Calculations for Decision Making in the United States: Characterization and Implications

T. Chakraborty[1], A. Hsu[2*], D. Manya[1], G. Sheriff[3]

[1]Yale School of Forestry and Environmental Studies, New Haven, CT, United States of America

[2]Yale-NUS College, Singapore

[3]School of Politics and Global Studies, Arizona State University, Tempe, AZ, United States of America

*Correspondence: angel.hsu@yale-nus.edu.sg

Abstract:

The urban heat island (UHI) effect is strongly modulated by urban-scale changes to the aerodynamic, thermal, and radiative properties of the Earth's land surfaces, and, among other things, exacerbates heat stress. With the majority (~80%) of the US population currently living in urban areas, urban heat stress is a threat to public health - one that will be aggravated by continuing urbanization, rural to urban migration, and climate change. While there have been hundreds of studies on the UHI, mostly done on a city-by-city basis, we do not have a complete picture at the national US scale using a consistent methodology, particularly regarding intra-city UHI variability. This within-city variability, caused by the spatial heterogeneity of urban areas may lead to higher heat exposure for certain vulnerable groups and is important for policy making and urban planning purposes. To address this gap, we characterize surface UHI intensities over the US using a modified Simplified Urban-Extent (SUE) approach by combining multiple US census-defined administrative urban delineations with a fusion of satellite products. We find the highest daytime UHI intensities during summer (mean value = 1.91 ± 0.97 °C) for 418 of 497 urbanized areas in the US, while the wintertime daytime UHI intensity (mean value = 0.87 ± 0.45 °C) is the lowest in 439 cases. Since urban vegetation has been frequently cited as an effective way to mitigate UHI, we use NDVI, a satellite-derived proxy for live green vegetation, and US census tract delineations to demonstrate that vegetation density strongly modulates inter-city, intra-city, and inter-seasonal variation in the UHI intensity. We use the census tract-based aggregation to demonstrate an application of this dataset, showing that for the majority of the urbanized areas, the UHI intensity is lower in census tracts with higher median income and higher proportion of white people. Moreover, poor and non-white urban residents seem to be suffering the adverse effects of summertime UHI without reaping the potential benefits during winter. We expect that this spatially explicit dataset, which can be explored here: https://datadrivenlab.users.earthengine.app/view/usuhiapp, can be directly implemented for policy making and urban planning, enabling the design of better mitigation strategies to ameliorate both the total UHI and disparities in its distribution.

1. Introduction

The urban heat island (UHI) effect refers to the phenomenon of higher temperatures in cities (Oke 1982), and from a public health perspective, can lead to, among other things, increased heat stress, heat strokes, dehydration, loss of productivity, and increased mortality among city-dwellers (Tan et al., 2010; Shahmohamadi et al., 2011; Heaviside et al., 2017). Both background climate (Zhao et al., 2014; Manoli et al., 2019) and city-specific characteristics, including the presence (or absence) of urban green space, amount (size of city), form (building height, ratio of building height to width of street canyon, etc.), and color (influencing reflectivity of solar radiation) of built-up structures, and intensity of human activity (through increased anthropogenic heat flux) (Peng et al. 2011), control the UHI's mean intensity and seasonal variability. The mean intensity and seasonal variability of the UHI are controlled by both the background climate the city is situated in, and the city-specific deviations from that base state (Zhao et al., 2014; Manoli et al., 2019). These deviations include presence (or absence) of urban green space, amount (size of city), form (building height, ratio of building height to width of street canyon, etc.), and color (influencing reflectivity of solar radiation) of built-up structures, and intensity of human activity (through increased anthropogenic heat flux) (Peng et al. 2011). In addition to these inter-city differences, the heterogeneity of urban areas leads to large intra-city variations in UHI intensity, which can result in different heat exposure for different demographic groups (Solecki et al., 2005; Jenerette et al., 2007). Previous studies have demonstrated that UHI exposure can be higher for poorer demographics across cities, an additional environmental stressor for already vulnerable populations (Chakraborty et al., 2019).

The UHI intensity can be calculated from either measurements of air temperature or satellite-derived surface temperature, termed the canopy and surface UHI, respectively, with potentially distinct diurnality and seasonality (Cui and Foi, 2012; Chakraborty et al., 2017). While the public health implications of urban heat exposure can be better captured using the canopy UHI, this assessment requires dense air temperature measurement networks in urban areas. Though these networks have become more common over time, measuring temperature in cities is rare (Muller et al., 2013). Moreover, using in-situ measurements suffers from considerations of representative placement, variable accuracy, and drift of individual sensors (Stewart 2011). On the other hand, many satellites have the advantage of monitoring all urban areas at the global scale using the same sensor. While this approach does not imply that they have no uncertainty, these uncertainties come from the selection of pixels to delineate urban and rural areas, as well as the higher uncertainty in satellite-derived products over heterogeneous urban terrain (Hulley et al., 2012; Vide et al., 2015; Zhang et al., 2019). Overall, using satellite observations allows us to compare the surface UHI intensity of different cities, as well as the intra-urban variations in the same, in a more consistent manner.

While there have been several multi-'city' studies on the UHI intensity from the national to the global scale (Peng et al., 2011; Clinton and Gong 2013; Li et al., 2017; Chakraborty and Lee 2019), the regions of interest in these analyses do not necessarily make them directly implementable from the policy making and urban planning perspective. Although the UHI effect stems from actual physical changes to the Earth's land surfaces, decision making aims to serve residents of administrative units. Chakraborty and Lee (2019) and Clinton and Gong (2013), for instance, both focus on urban agglomerations, not cities administrative boundaries, which limit their application for policymakers who are interested in designing UHI mitigation strategies for urban residents. For global studies, comparing

UHI intensities using administratively determined city delineations is problematic since city definitions vary widely across contexts.

To address these gaps in UHI comparability and utility for policy applications, here we focus on the United States and US Census-defined administrative boundaries to create a methodologically consistent characterization of UHI intensity, to provide actionable results for urban planners and policy makers. Using satellite observations, we characterize annual, summertime, and wintertime UHI intensities across different climate zones and examine how urban vegetation modulates the intra-city and inter-city variability in UHI intensity. By focusing on only US cases, we can compare cities with similar sociocultural backgrounds using relatively consistent administrative units of calculation, which are based on the general distribution of demographic groups. As a demonstration of the relevance of this dataset, we provide preliminary evidence of the large disparities in UHI exposure for different income and racial groups in the US, which are discussed in more detail in Hsu et al (Under Review). Our results have important implications for understanding and managing urban heat exposure in the US, particularly for vulnerable populations, and can inform urban-scale policymaking for climate adaptation in an increasingly urban and warmer world.

2. Methodology

2.1 Data Sources and Regions of Interest

We use the following remotely sensed data in the present study:
1. The Moderate Resolution Imaging Spectroradiometer (MODIS) 8-day Land Surface Temperature (LST) product from NASA's Aqua satellite (MYD11A2 v006) at 1000 m resolution from 2013 to 2017 (Wan 2014)
2. MODIS 8-day surface reflectance product from Aqua satellite (MYD09A1 v006) at 500 m resolution from 2013 to 2017 (Vermote et al., 2011)
3. Global Multi-Resolution Terrain Elevation Data (GMTED) at 30 m resolution from 2010 (Danielson and Gesch, 2011)
4. European Space Agency's Climate Change Initiative (ESA CCI) land cover data at 300 m resolution for 2015 (Bontemps et al., 2005)

Measurements from the MODIS sensor on the Aqua satellite are chosen over the Terra satellite since the overpass time during the day for Aqua is 1:30 pm local time, which better corresponds to the peak daytime temperature. We combine satellite data with socioeconomic data for census tracts from the American Community Survey (Mather et al., 2005). Since the focus is on urban areas, we only consider the census tracts intersecting urbanized areas for 2010, which the US census bureau defines as densely settled geographical regions with more than 50,000 residents (https://www.census.gov/programs-surveys/geography/guidance/geo-areas/urban-rural/2010-urban-rural.html). A total of 55,871 census tracts are considered, grouped into 497 urbanized areas (Figs 1 and 2). For these census tracts, median household income, and demographic information by race (particularly White, Black, Asian, American Indian, Hawaiian, and others) from American Community Survey 5-year Data Profile from 2017 (US Census Bureau 2018) are used to demonstrate the disparities in UHI exposure as a use case for the UHI database.

The prevailing background climate for each urbanized area is determined from the Koppen Geiger dataset (Rubel and Kottek, 2010), based on the climate zone of the centroid of each of the chosen 497 census tract groups. Finally, each census tract group is considered coastal if the original urbanized area intersects the Natural Earth global coastal dataset at 10 m resolution (https://www.naturalearthdata.com/downloads/10m-physical-vectors/10m-coastline/). All spatial analyses are done on the Google Earth Engine platform (Gorelick et al., 2017).

2.2 Satellite Data processing

We pre-processed the LST images to only include pixels with an uncertainty of less than or equal to 3 K, similar to Chakraborty and Lee (2019). We also use the MODIS surface reflectance product to compute the Normalized Difference Vegetation Index (NDVI) (Rouse et al., 1974) using the highest quality pixels using the equation:

NDVI = (NIR-RED)/(NIR+RED)

Where NIR and RED are the surface reflectances in the near infrared (band 2) and red (band 1), respectively. Finally, terrain elevation is calculated by extracting the Digital Elevation Model (DEM) values from Danielson and Gesch (2011).

For both LST and NDVI, the annual values are the simple means of all the images, while the summertime and wintertime values are the means of the images from June to August and December to February, respectively. DEM has no seasonal component and is thus just a static value. We use the ESA CCI land cover data for 2015 since it is in the middle of the 2013 to 2017 range. All satellite data are processed at 300 m resolution to be consistent with the land cover data.

2.3 UHI and Urban-Rural Differential Estimation at Multiple Levels of Aggregation

We use the Simplified Urban Extent (SUE) algorithm, originally developed to characterize surface UHI intensity in a globally consistent manner (Chakraborty and Lee, 2019), to calculate the annual, summertime, and wintertime surface UHI intensities for day and night. Traditional UHI estimates usually assume a fixed buffer around an urban region of interest to create a rural reference and compare the temperature differential between the two (Clinton and Gong, 2013). However, the footprint of the UHI can vary widely between cities (Zhou et al., 2015; Yang et al., 2019), preventing a standard method to select a rural reference based on these buffers. This is an even bigger issue when using administrative boundaries since the region around these may or may not be built-up. The SUE method defines the UHI as the average LST difference between the urban and non-urban pixels, as classified from spectral reflectance data, within an urban agglomeration or city (Chakraborty and Lee, 2019). This essentially denotes the average surface temperature change as people move from non built-up to built-up regions within the agglomeration. The results from the SUE algorithm have been independently validated against both observational and theoretical estimates of UHI intensity (Manoli et al., 2020; Niu et al., 2020).

In the present study, we use the US Census Bureau's 497 urbanized areas, representing roughly 78 percent of the total population, as the urban agglomerations, while the ESA CCI pixel-level data are used to delineate urban and rural references. Thus, the rural reference includes all non-urban, non-

water land cover classes within the regions of interest. The UHI is the mean temperature difference between the urban pixels and the rural reference pixels, separately calculated for each urbanized area. Similar to the UHI, we also calculate urban-rural differentials of NDVI (ΔNDVI) and DEM (ΔDEM) for each agglomeration.

To calculate the UHI and urban-rural differentials for a census tract, we keep the rural reference identical (based on the non-urban, non-water ESA CCI pixels within the urbanized area), while all pixels within the urbanized part of the census tracts are used as the urban reference. This is a necessary modification to the SUE algorithm to account for the mismatch between the physical extent of an urban area and its administrative boundaries (Hsu et al., 2018; Chakraborty et al., 2019). While this does not keep both remotely sensed and socioeconomic data at the same level of aggregation, we assume that most of the people living in census tracts that cross the boundaries of the urbanized areas live in the urbanized part. Moreover, using all pixels within the census tract gives a more complete picture of the average surface temperature of the tract, accounting for presence (or absence) of green space, bare soil, permanent snowpack, etc. Figure 1 shows two examples of these two different levels of aggregation used in the present study.

3. Results

3.1 Spatial and Seasonal Variability in Surface UHI in the US

Figure 2 shows a map of US urbanized areas including their mean annual daytime and nighttime surface UHI intensities. The annual average surface UHI intensity is 1.38 ± 0.66 °C during daytime and 0.40 ± 0.28 °C for nighttime. Seasonally, summers show the highest values (1.91 ± 0.97 °C for daytime; 0.60 ± 0.26 °C for nighttime), while winters show the lowest (0.87 ± 0.45 °C for daytime; 0.31 ± 0.34 °C at night; Table 1). The summertime UHI is higher than the annual mean UHI in ~84% (418/497) of the cases, while the wintertime UHI is higher in only ~12% (58/497) cases. This seasonal trend of higher summertime UHI intensities compared to wintertime values is consistent with previous results - both global and US-specific (Imhoff et al., 2010; Peng et al., 2011; Debbage and Shephard 2015; Li et al., 2017; Chakraborty and Lee 2019), and show similar magnitude to the 15-year mean urban cluster-based values extracted from the dataset created by Chakraborty and Lee (2019) (Table 2). Note that the slightly higher UHI values in the present study are due to primarily two reasons:
1. The global dataset uses a fusion of Terra and Aqua data, with Aqua, which we use in the present study, generally showing higher daytime UHI values (Chakraborty and Lee 2019).
2. We focus on urbanized areas, and thus filter out many smaller urban areas with lower expected UHI values (Oke 1967).

When divided into climate classes, there is a marked difference in daytime UHI intensity between arid and other climate zones. Arid cities show the lowest UHI intensities while tropical cities show the highest, both with little seasonal variation. Temperate and boreal cities show larger seasonal variations. Arid zones also show the lowest within-city spatial variation in daytime UHI intensity for all cases (Fig. 3). During nighttime, cities in arid climate show the highest surface UHI intensity (Fig. 3b).

While these trends are consistent with global patterns, some results are affected by the US-specific characteristics of urbanization. With a primarily continental climate, the US contains 298 temperate urbanized areas, with only 16 in tropical climate, most of which are on islands, either in Hawaii or Puerto

Rico. The average UHI intensities are thus skewed by values in the temperate zone. Moreover, since only one of the 44 arid urbanized areas, San Diego, CA, adjoins the coast, the low UHI intensity in arid areas leads to a higher overall annual UHI intensity for coastal urbanized areas (1.46 ± 0.77 °C for coastal; 1.36 ± 0.63 °C for non-coastal), which is counter-intuitive, given the moderating influence of sea breezes on daytime coastal temperature. The expected pattern emerges when this analysis is done separately for temperate (1.36 ± 0.68 °C for coastal; 1.40 ± 0.55 °C for non-coastal) and boreal (1.25 ± 0.54 °C for coastal; 1.56 ± 0.60 °C for non-coastal) urbanized areas. This result is mostly consistent for summertime and wintertime UHI intensities (Table 1). During nighttime, where one would expect coastal cities to have relatively higher temperatures, summertime UHI intensity is actually higher for non-coastal cities (0.53 ± 0.31 °C for coastal; 0.62 ± 0.25 °C for non-coastal). This difference is not due to a sampling issue since we essentially analyze the entire population of urbanized areas, as defined by the US census bureau, in the present study, covering ~78% of US residents. While it is possible to extend this analysis to the urban areas, which the US census bureau defines as regions with a population of less than 50,000 people, some of these tend to be very small and have very few census tracts, making the sample sizes too small for the equity example shown below or to get enough representative pixels to reliably calculate the UHI intensity.

3.2 UHI Intensity and Urban Green Space

A major contributor to UHI intensity, particularly its intra-city variation, is the presence (or absence) of urban vegetation. While this is one of many factors that control the UHI (Peng et al., 2011; Zhao et al., 2014), we focus on it due to its significant intra-city and inter-city variation (Chakraborty et al. 2019), since access to green space has previously been found to be inversely correlated with income (Hsu et al., 2018; Nesbitt et al. 2019; Chakraborty et al. 2019), and because it is often proposed as one of the main UHI mitigation strategies (Cui and De Foy, 2012; Ziter et al. 2019). Moreover, the presence of green vegetation has other co-benefits beyond reducing local temperature (Dadvand et al. 2015; Fong et al. 2018; Engemann et al. 2019; Iyer et al. 2020). Given the multiple economic and social benefits of urban forestry (Nowak and Dwyer, 2007), planting urban trees can be an easily implementable and defensible from the policy standpoint.

Daytime surface UHI intensity and the urban-rural differential in NDVI (ΔNDVI), a proxy for live green vegetation, are negatively correlated both within cities and between cities (Fig. 4), except for the boreal climate. These correlations are especially strong during summer, which is expected due to higher potential evaporative cooling from vegetated surfaces during this season (Manoli et al. 2020). Overall, the negative correlations persist for 459, 481, and 368 of the 497 urbanized areas for the year, summertime, and wintertime, respectively. The correlations are stronger for non-coastal cities than for coastal cities (annually, r=-0.42 ± 0.45 for coastal cities and -0.66 ± 0.45 for non-coastal cities after Fisher's z transformation and back-transformation). This difference is due to the mediating effect of sea breezes in coastal cities and suggests that increasing green space may not be as effective at reducing the disparity in heat exposure in these cities. For temperate climate, which has a large number of both coastal and inland cities, the difference in correlations between coastal and non-coastal urbanized areas is even stronger (annually, r=-0.41 ± 0.46 for coastal cities and -0.75 ± 0.38 for non-coastal cities), particularly for summer (r=-0.50 ± 0.46 for coastal cities and -0.80 ± 0.36 for non-coastal cities). Given the overall stronger correlation between summertime surface UHI and summertime ΔNDVI, this mitigation option is more efficient during this seasonal temperature peak.

Although the overall trends persist during nighttime (Figs 4d, 4e, and 4f), the strengths of the negative correlations are much lower, expected due to the lower differential of (and absolute) evaporative cooling at night (Dios et al. 2015). In particular, at night, the control of ΔNDVI on inter-city variation in UHI practically disappears. A negative trend in UHI and ΔNDVI is found in 400, 456, and 319 urbanized areas for the year, summertime, and wintertime, respectively and the correlations for non-coastal cities decrease the most to -0.32 ± 0.37 (r=-0.40 ± 0.38 for coastal cities).

3.3 Applications of Dataset: Exploring UHI Exposure by Income and Race

In a recent study, we demonstrated that UHI exposure is higher in poorer neighborhoods for the majority of a sample of 25 global cities (Chakraborty et al., 2019). We also found that, while UHI intensity tends to be higher in the urban core in most cases, segregation of people from different income groups explains the distribution of heat exposure. Recent studies have explored the distribution of environmental stressors and access to resources for different socioeconomic groups in the US (Clark et al., 2014; Stokes and Seto, 2018; Tessum et al., 2019; Hoffman et al., 2020). Here, we demonstrate uses of this dataset relevant to this line of research by exploring the statistical associations between UHI intensity, income and race.

Expanding on the analysis done by Chakraborty et al. (2019), we show the statistical relationship between UHI intensity and median income for all urbanized areas (Fig. 5). UHI intensity is negatively associated with median income for 436 (~88%), 445 (~89%), and 428 (~86%) of the 497 urbanized areas during the year, summer, and winter, respectively. For all seasons, the strengths of the correlations are highest for the boreal climate, followed by temperate and arid climate. The correlations for the tropical cities show a fairly even spread from negative to positive. Nighttime UHI intensity also shows negative, albeit weaker, correlations with median income (Figs 5d, 5e, and 5f). While the daytime UHI is more relevant for heat strokes, previous studies have shown that high nighttime temperatures can also increase mortality, especially due to chronic exposure (Laaidi et al., 2012). On the other hand, the UHI can also potentially reduce cold waves (Oleson et al., 2018) - an important factor to consider when comparing UHI mitigation strategies, particularly in colder climates where cold snaps, rather than heat waves, are the more public-health relevant concern. More importantly, the canopy UHI, which is direct cause of urban heat stress, is generally much higher at night, especially in the US (Zhang et al. 2014). Satellite data, as used in the present study, may overestimate the actual UHI exposure, as well the intra-city differentials for population groups, which is a major limitation of satellite-based UHI quantification in the context of public health.

Similarly, for the majority of the urbanized areas, the mean daytime UHI intensity is negatively correlated with the percentage of white population, meaning census tracts with higher proportion of white residents have lower exposure to UHI (Fig. 6 shows the patterns for summer). Overall, white is the only racial group for which the mean correlation between UHI intensity and proportion of population is negative, while the mean positive correlation is highest for the black racial group. These patterns persist even after accounting for income, as seen from the distribution of partial correlation coefficients between the two variables (Fig. 6b). For winter nights, the association between UHI intensity and race practically disappears (Fig. 6c), especially after accounting for income (Fig. 6d).

4. Discussion

4.1 Census-tract Elevation: A Possible Confounding Factor

Since temperature varies with altitude, comparing UHI intensities at different elevations is not ideal. In the UHI literature, this is accounted for by setting elevation differential thresholds for entire cities (for multi-city analysis) or for individual pixels before calculating the UHI. However, with the aim of looking at exposure to urban heat, it is not necessary that higher elevation areas will not be inhabited. Moreover, since we are constrained by the US Census definitions to create a UHI dataset consistent with administrative boundaries, using such a threshold would mask out entire census tracts or large parts of the population who live in higher elevation regions of the urbanized areas. Thus, for the sake of consistent exposure assessment, we do not use elevation thresholds, acknowledging that this would lead to some uncertainties in urbanized areas with large terrain gradients. For the purpose of illustration, we examine the relationship between UHI intensity and the urban-rural elevation differential (ΔDEM) for each urbanized area (Fig. 7). The elevation differential is indeed important, showing a negative correlation with UHI intensity for a slight majority of the urbanized areas considered. While there is not as much inter-seasonal trend, roughly two-thirds of urbanized areas (316 for year, 320 for summer, and 342 for winter) demonstrate this negative correlation, confirming that census tracts with a higher average elevation have lower temperature, though we should be a bit more cautious about calling it an UHI intensity in this context. The negative correlations are slightly lower at night.

4.2 UHI Intensity, Urban Vegetation, and Population Distributions

While the UHI intensity is typically higher for the urban core, income distribution within cities depends strongly on sociocultural context. For the US, this distribution is partly a result of a history of urban and national-scale policy-making, and stems from, among other things, predominance of urban flight, redlining policies, and access to public transportation (Kahn et al., 2008; Hoffman et al., 2020). Here we demonstrate an example case of disparity in UHI intensity for a single nation, thus partly controlling for the variabilies in those sociocultural factors. Physical factors may also control the disparity in UHI exposure, particularly urban vegetation (Chakraborty et al, 2019; Nesbitt et al., 2019). We see positive correlations between ΔNDVI and median income (Fig. 8a, 8b, and 8c), implying richer urban residents live in 'greener' census tracts. However, for coastal cities, we see weaker correlations between ΔNDVI and median income (r=0.28 ± 0.30 for coastal cities and -0.45 ± 0.29 for non-coastal cities for the year; r=0.27 ± 0.30 for coastal cities and -0.46 ± 0.30 for non-coastal cities for summer), which is not surprising since ocean-adjacent census tracts, which may have less vegetation cover, generally house richer populations. We separated the difference in summertime and wintertime NDVI for the low income tracts (below 25 percentile of income) and high income tracts (above 75 percentile of income) for each urbanized area (Fig. 8d). We find that this mean difference (of summer NDVI-winter NDVI) is greater in high income tracts for temperate and boreal climate zones (p<0.01), but not for arid and tropical climate. This is due to the stronger vegetation phenology in temperate and boreal climate due to the larger abundance of deciduous trees and shrubs. Similar values in the difference in summertime and wintertime NDVI in both low income and high income tracts for tropical and arid cases explain the practically non-varying relationships between daytime UHI intensity and median income for cities in these climate zones. Similarly, the difference between summertime and wintertime NDVI is significantly (p<0.01) higher for white-dominant tracts (over 75% white residents) than non-white dominant tracts (under 25% white residents) for temperate and boreal climate.

4.3 Limitations and Implications

Though surface temperature and air temperature are correlated at the annual scale, the seasonal trends may be different (Chakraborty et al. 2017). Moreover, while air temperature is an important environmental stressor, heat stress also depends on other factors, including humidity, wind speed, and radiation (Oleson et al. 2015). Unfortunately, at the moment, there are not enough measurements of air temperature inside city boundaries, let alone other variables needed to predict heat stress at high resolution, making such cross-city comparisons of urban heat stress difficult. Moreover, the UHI is not an environmental stressor under all circumstances, since in some cases, especially in boreal climate and at night, a higher temperature may be preferable (Yang and Bou-Zeid, 2018). As we note from Fig. 5, the negative association between UHI and median income is much weaker at night, practically disappearing during winter. Since we can reasonably assume that the UHI has negative health effects during summer days and positive health effects during winter nights, our results imply that poor people may be suffering the adverse effects of UHI without reaping the potential wintertime benefits. This result holds for race as well, with lower potential UHI intensity for white-dominant census tracts during summer days and a relatively even distribution of UHI intensity regardless of race for winter nights (Fig. 6). Moving beyond the public health consequences, since the UHI reduces heating demand during winter and increases cooling demand during summer (Santamouris, 2014), poor and non-white people in the US are disproportionately bearing the economic burden of the UHI during both seasons. Evident from Fig. 8, these seasonal trends in UHI disparity are particularly relevant for boreal and temperate cities in the US. These city-specific variabilities need to be taken into account when planning UHI mitigation strategies, both to reduce the mean UHI of the city, and to address environmental disparities in UHI exposure within cities and across seasons. The methodologically consistent UHI dataset generated in this study is constrained by US census-defined urbanized areas, which, from an administrative standpoint, makes it ideal for developing these strategies.

Computational limits aside, it is possible to use higher resolution thermal images, for instance Landsat (Jiménez-Muñoz et al., 2014), to characterize UHI for even smaller census-defined administrative areas, like census block groups. Since we can have significant variabilities within census tracts, especially for cities with lower population density, this would allow us to further uncover the true distribution of surface UHI within the US. However, in the present study, we use the MODIS sensor since, even though the data are coarser than Landsat, MODIS has the advantage of more frequent return periods, reducing possible biases due to cloud cover, and is also available at night, which is important, albeit less studied, for examining both the economic and health impacts of the UHI effect (Laaidi et al., 2012; Santamouris, 2014; Oleson et al. 2015; Heaviside et al., 2017).

5. Conclusions

Most urban heat island characterizations are done using physical delineations of urban areas and their rural references. While this is ideal since urban heat islands are primarily due to changes in the physical characteristics of the land surface, the mismatch between physical boundaries and administrative boundaries makes comparisons between and within cities difficult, especially for decision making. Here, we use multiple administrative boundary definitions and a fusion of satellite products to characterize the intra and inter-city variation in the annual, summertime, and wintertime UHI intensities during daytime and nighttime in the US. Our results converge with previous, physical-

boundary based estimates and can be used to separate UHI intensity at the census tract level to examine disparities in heat exposure across demographic groups in the US. We demonstrate that the UHI intensity is negatively correlated with income and percentage of white population and that poor and non-white urban residents tend to be exposed to higher summer daytime UHI, when heat stress is at its maximum, and similar winter nighttime UHI, when poorer residents could potentially benefit from higher ambient temperatures. We also demonstrate that UHI intensity, its seasonality, and spatial variability are strongly associated with the degree of vegetation cover in and within cities. Thus, strategically placing urban parks and green spaces can be a useful way to reduce both the mean UHI, as well as its spatial variability, thus mitigating heat exposure for vulnerable populations across seasons. Our data can be accessed through this web application: https://datadrivenlab.users.earthengine.app/view/usuhiapp and will hopefully be useful for planning UHI mitigation strategies in the US.

Acknowledgements

References:

1. Bontemps S, Defourny P, Radoux J, Van Bogaert E, Lamarche C, Achard F and Zülkhe M 2013 Consistent global land cover maps for climate modelling communities: current achievements of the ESA's land cover CCI *Proc. ESA Living Planet Symp.* pp 9–13

2. Chakraborty T and Lee X 2019 A simplified urban-extent algorithm to characterize surface urban heat islands on a global scale and examine vegetation control on their spatiotemporal variability *Int. J. Appl. Earth Obs. Geoinf.* 74 269–80

3. Chakraborty, T., Hsu, A., Manya, D., & Sheriff, G. (2019). Disproportionately higher exposure to urban heat in lower-income neighborhoods: a multi-city perspective. *Environmental Research Letters*, *14*(10), 105003.

4. Chakraborty, T., Sarangi, C., & Tripathi, S. N. (2017). Understanding diurnality and inter-seasonality of a sub-tropical urban heat island. *Boundary-Layer Meteorology*, *163*(2), 287-309.

5. Clark, L. P., Millet, D. B., & Marshall, J. D. (2014). National patterns in environmental injustice and inequality: outdoor NO2 air pollution in the United States. *PloS one*, *9*(4), e94431.

6. Clinton, N., & Gong, P. (2013). MODIS detected surface urban heat islands and sinks: Global locations and controls. *Remote Sensing of Environment*, *134*, 294-304.

7. Cui, Y. Y., & De Foy, B. (2012). Seasonal variations of the urban heat island at the surface and the near-surface and reductions due to urban vegetation in Mexico City. *Journal of Applied Meteorology and Climatology*, *51*(5), 855-868.

8. Dadvand, P., Nieuwenhuijsen, M. J., Esnaola, M., Forns, J., Basagaña, X., Alvarez-Pedrerol, M., ... & Jerrett, M. (2015). Green spaces and cognitive development in primary schoolchildren. *Proceedings of the National Academy of Sciences*, *112*(26), 7937-7942.

9. Danielson, J. J., & Gesch, D. B. (2011). *Global multi-resolution terrain elevation data 2010 (GMTED2010)* (p. 26). US Department of the Interior, US Geological Survey.

10. De Dios, V. R., Roy, J., Ferrio, J. P., Alday, J. G., Landais, D., Milcu, A., & Gessler, A. (2015). Processes driving nocturnal transpiration and implications for estimating land evapotranspiration. *Scientific reports*, *5*, 10975.

11. Debbage, N., & Shepherd, J. M. (2015). The urban heat island effect and city contiguity. *Computers, Environment and Urban Systems*, *54*, 181-194.

12. Engemann, K., Pedersen, C. B., Arge, L., Tsirogiannis, C., Mortensen, P. B., & Svenning, J. C. (2019). Residential green space in childhood is associated with lower risk of psychiatric disorders from adolescence into adulthood. *Proceedings of the National Academy of Sciences*, *116*(11), 5188-5193.

13. Fong, K. C., Hart, J. E., & James, P. (2018). A review of epidemiologic studies on greenness and health: Updated literature through 2017. Current environmental health reports, 5(1), 77-87.

14. Gorelick, N., Hancher, M., Dixon, M., Ilyushchenko, S., Thau, D., & Moore, R. (2017). Google Earth Engine: Planetary-scale geospatial analysis for everyone. *Remote Sensing of Environment*, *202*, 18-27.

15. Heaviside, C., Macintyre, H., & Vardoulakis, S. (2017). The Urban Heat Island: implications for health in a changing environment. *Current environmental health reports*, *4*(3), 296-305.

16. Hoffman, J. S., Shandas, V., & Pendleton, N. (2020). The Effects of Historical Housing Policies on Resident Exposure to Intra-Urban Heat: A Study of 108 US Urban Areas. *Climate*, *8*(1), 12.

17. https://www.census.gov/programs-surveys/geography/guidance/geo-areas/urban-rural/2010-urban-rural.html

18. https://www.naturalearthdata.com/downloads/10m-physical-vectors/10m-coastline/

19. Hsu, A., Alexandre, N., Brandt, J., Chakraborty, T., Comess, S., Feierman, A., ... & Moyo, N. (2018). The Urban Environment and Social Inclusion Index. *New Haven, CT: Yale University. Available: datadrivenlab. org/urban*.

20. Hsu, A., Chakraborty, T., Sheriff, G., Manya, D. (Under Review). Disparities in Urban Heat Island Exposure: Summer Daytime Distribution by Race and Income in Major U.S. Cities

21. Hulley, G. C., Hughes, C. G., & Hook, S. J. (2012). Quantifying uncertainties in land surface temperature and emissivity retrievals from ASTER and MODIS thermal infrared data. *Journal of Geophysical Research: Atmospheres*, *117*(D23).

22. Imhoff, M. L., Zhang, P., Wolfe, R. E., & Bounoua, L. (2010). Remote sensing of the urban heat island effect across biomes in the continental USA. *Remote sensing of environment*, *114*(3), 504-513.

23. Iyer, H. S., Valeri, L., James, P., Chen, J. T., Hart, J. E., Laden, F., ... & Rebbeck, T. R. (2020). The contribution of residential greenness to mortality among men with prostate cancer: a registry-based cohort study of Black and White men. *Environmental Epidemiology*, *4*(2), e087.

24. Jenerette, G. D., Harlan, S. L., Brazel, A., Jones, N., Larsen, L., & Stefanov, W. L. (2007). Regional relationships between surface temperature, vegetation, and human settlement in a rapidly urbanizing ecosystem. *Landscape ecology*, *22*(3), 353-365.

25. Jiménez-Muñoz, J. C., Sobrino, J. A., Skoković, D., Mattar, C., & Cristóbal, J. (2014). Land surface temperature retrieval methods from Landsat-8 thermal infrared sensor data. *IEEE Geoscience and remote sensing letters*, *11*(10), 1840-1843.

26. Kahn, M. E., Glaeser, E., & Rappaport, J. (2008). Why do the poor live in cities? The role of public transportation.

27. Laaidi, K., Zeghnoun, A., Dousset, B., Bretin, P., Vandentorren, S., Giraudet, E., & Beaudeau, P. (2012). The impact of heat islands on mortality in Paris during the August 2003 heat wave. *Environmental health perspectives*, *120*(2), 254-259.

28. Li, X., Zhou, Y., Asrar, G. R., Imhoff, M., & Li, X. (2017). The surface urban heat island response to urban expansion: A panel analysis for the conterminous United States. *Science of the Total Environment*, *605*, 426-435.

29. Manoli, G., Fatichi, S., Bou-Zeid, E., & Katul, G. G. (2020). Seasonal hysteresis of surface urban heat islands. *Proceedings of the National Academy of Sciences*.

30. Manoli, G., Fatichi, S., Schläpfer, M., Yu, K., Crowther, T. W., Meili, N., ... & Bou-Zeid, E. (2019). Magnitude of urban heat islands largely explained by climate and population. *Nature*, *573*(7772), 55-60.

31. Martin-Vide, J., Sarricolea, P., & Moreno-García, M. C. (2015). On the definition of urban heat island intensity: the "rural" reference. Frontiers in Earth Science, 3, 24.

32. Mather, M., Rivers, K. L., & Jacobsen, L. A. (2005). The American Community Survey. *Population Bulletin*, *60*(3), 1-20.

33. Muller, C. L., Chapman, L., Grimmond, C. S. B., Young, D. T., & Cai, X. (2013). Sensors and the city: a review of urban meteorological networks. *International Journal of Climatology*, *33*(7), 1585-1600.

34. Nesbitt, L., Meitner, M. J., Girling, C., Sheppard, S. R., & Lu, Y. (2019). Who has access to urban vegetation? A spatial analysis of distributional green equity in 10 US cities. *Landscape and Urban Planning*, *181*, 51-79.

35. Niu, L., Tang, R., Jiang, Y., & Zhou, X. (2020). Spatiotemporal Patterns and Drivers of the Surface Urban Heat Island in 36 Major Cities in China: A Comparison of Two Different Methods for Delineating Rural Areas. *Sustainability*, *12*(2), 478.

36. Nowak, D. J., & Dwyer, J. F. (2007). Understanding the benefits and costs of urban forest ecosystems. In *Urban and community forestry in the northeast* (pp. 25-46). Springer, Dordrecht.

37. Oke, T. R. (1982). The energetic basis of the urban heat island. *Quarterly Journal of the Royal Meteorological Society*, *108*(455), 1-24.

38. Oke, Tim R. "City size and the urban heat island." *Atmospheric Environment (1967)* 7.8 (1973): 769-779.

39. Oleson, K. W., Monaghan, A., Wilhelmi, O., Barlage, M., Brunsell, N., Feddema, J., ... & Steinhoff, D. F. (2015). Interactions between urbanization, heat stress, and climate change. *Climatic Change*, *129*(3-4), 525-541.

40. Oleson, K. W., Anderson, G. B., Jones, B., McGinnis, S. A., & Sanderson, B. (2018). Avoided climate impacts of urban and rural heat and cold waves over the US using large climate model ensembles for RCP8. 5 and RCP4. 5. *Climatic change*, *146*(3-4), 377-392.

41. Peng, S., Piao, S., Ciais, P., Friedlingstein, P., Ottle, C., Bréon, F. M., ... & Myneni, R. B. (2011). Surface urban heat island across 419 global big cities.

42. Rouse J Jr, Haas R H, Schell J A and Deering D W 1974 Monitoring vegetation systems in the Great Plains with ERTS *NASA Goddard Space Flight Center 3DERTS-1 Symp.* vol 1 pp 309–17 section A

43. Rubel F and Kottek M 2010 Observed and projected climate shifts 1901–2100 depicted by world maps of the Köppen-Geiger climate classification *Meteorol. Z.* 19 135–41

44. Santamouris, M. (2014). On the energy impact of urban heat island and global warming on buildings. *Energy and Buildings*, *82*, 100-113.

45. Shahmohamadi, P., Che-Ani, A. I., Etessam, I., Maulud, K. N. A., & Tawil, N. M. (2011). Healthy environment: the need to mitigate urban heat island effects on human health. *Procedia Engineering*, *20*, 61-70.

46. Solecki, W. D., Rosenzweig, C., Parshall, L., Pope, G., Clark, M., Cox, J., & Wiencke, M. (2005). Mitigation of the heat island effect in urban New Jersey. *Global Environmental Change Part B: Environmental Hazards*, *6*(1), 39-49.

47. Stewart, I. D. (2011). A systematic review and scientific critique of methodology in modern urban heat island literature. *International Journal of Climatology*, *31*(2), 200-217.

48. Stokes, E. C., & Seto, K. C. (2018). Tradeoffs in environmental and equity gains from job accessibility. *Proceedings of the National Academy of Sciences*, *115*(42), E9773-E9781.

49. Tan, J., Zheng, Y., Tang, X., Guo, C., Li, L., Song, G., ... & Chen, H. (2010). The urban heat island and its impact on heat waves and human health in Shanghai. *International journal of biometeorology*, *54*(1), 75-84.

50. Tessum, C. W., Apte, J. S., Goodkind, A. L., Muller, N. Z., Mullins, K. A., Paolella, D. A., ... & Hill, J. D. (2019). Inequity in consumption of goods and services adds to racial–ethnic disparities in air pollution exposure. *Proceedings of the National Academy of Sciences*, *116*(13), 6001-6006.

51. Vermote, E. F., Kotchenova, S. Y., & Ray, J. P. (2011). MODIS surface reflectance user's guide. *MODIS Land Surface Reflectance Science Computing Facility, version*, *1*.

52. Wan, Zhengming. "New refinements and validation of the collection-6 MODIS land-surface temperature/emissivity product." *Remote sensing of Environment* 140 (2014): 36-45.

53. Yang, J., & Bou-Zeid, E. (2018). Should cities embrace their heat islands as shields from extreme cold?. *Journal of Applied Meteorology and Climatology*, *57*(6), 1309-1320.

54. Yang, Q., Huang, X., & Tang, Q. (2019). The footprint of urban heat island effect in 302 Chinese cities: Temporal trends and associated factors. *Science of The Total Environment*, *655*, 652-662.

55. Zhang, P., Bounoua, L., Imhoff, M. L., Wolfe, R. E., & Thome, K. (2014). Comparison of MODIS land surface temperature and air temperature over the continental USA meteorological stations. *Canadian Journal of Remote Sensing*, *40*(2), 110-122.

56. Zhang, Q., Zhang, M., Zhou, W., Xu, W., & Zhang, J. (2019, July). The Influence of Different Urban and Rural Selection Methods on the Spatial Variation of Urban Heat Island Intensity. In *IGARSS 2019-2019 IEEE International Geoscience and Remote Sensing Symposium* (pp. 4403-4406). IEEE.

57. Zhao, L., Lee, X., Smith, R. B., & Oleson, K. (2014). Strong contributions of local background climate to urban heat islands.

58. Zhou, D., Zhao, S., Zhang, L., Sun, G., & Liu, Y. (2015). The footprint of urban heat island effect in China. *Scientific reports*, *5*, 11160.

59. Ziter, C. D., Pedersen, E. J., Kucharik, C. J., & Turner, M. G. (2019). Scale-dependent interactions between tree canopy cover and impervious surfaces reduce daytime urban heat during summer. *Proceedings of the National Academy of Sciences*, *116*(15), 7575-7580.
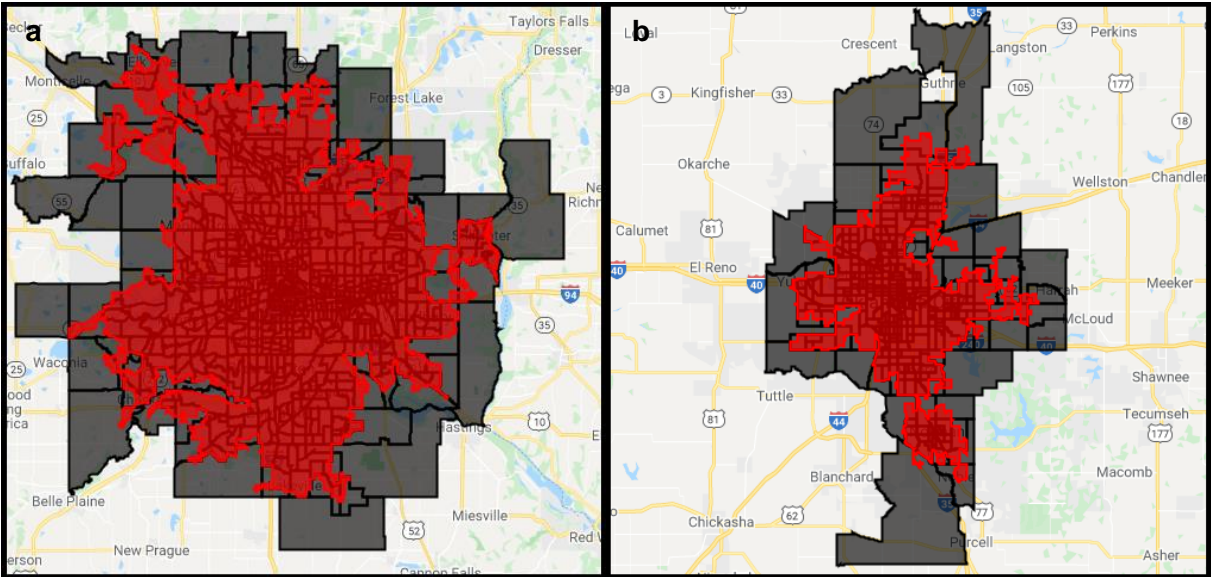

Fig. 1 Examples of the two levels of aggregation used for processing the satellite data for **(a)** Minneapolis, Minnesota and **(b)** Oklahoma City, Oklahoma. The red polygons are the urbanized areas

used for calculating city-specific UHI intensity by separately calculating LST over spectrally classified urban and rural references. The black polygons show the groups of census tracts that overlap with the urbanized areas for each case. Only the satellite data over the urbanized areas are used for calculations. Thus, while the values for the inner-city census tracts are the same as the average over the whole tract, for the census tracts extending beyond the edge of the urbanized areas, only the pixels in the urbanized portion are considered to calculate census tract-level UHI intensity. Data can be visualized here: https://datadrivenlab.users.earthengine.app/view/usuhiapp
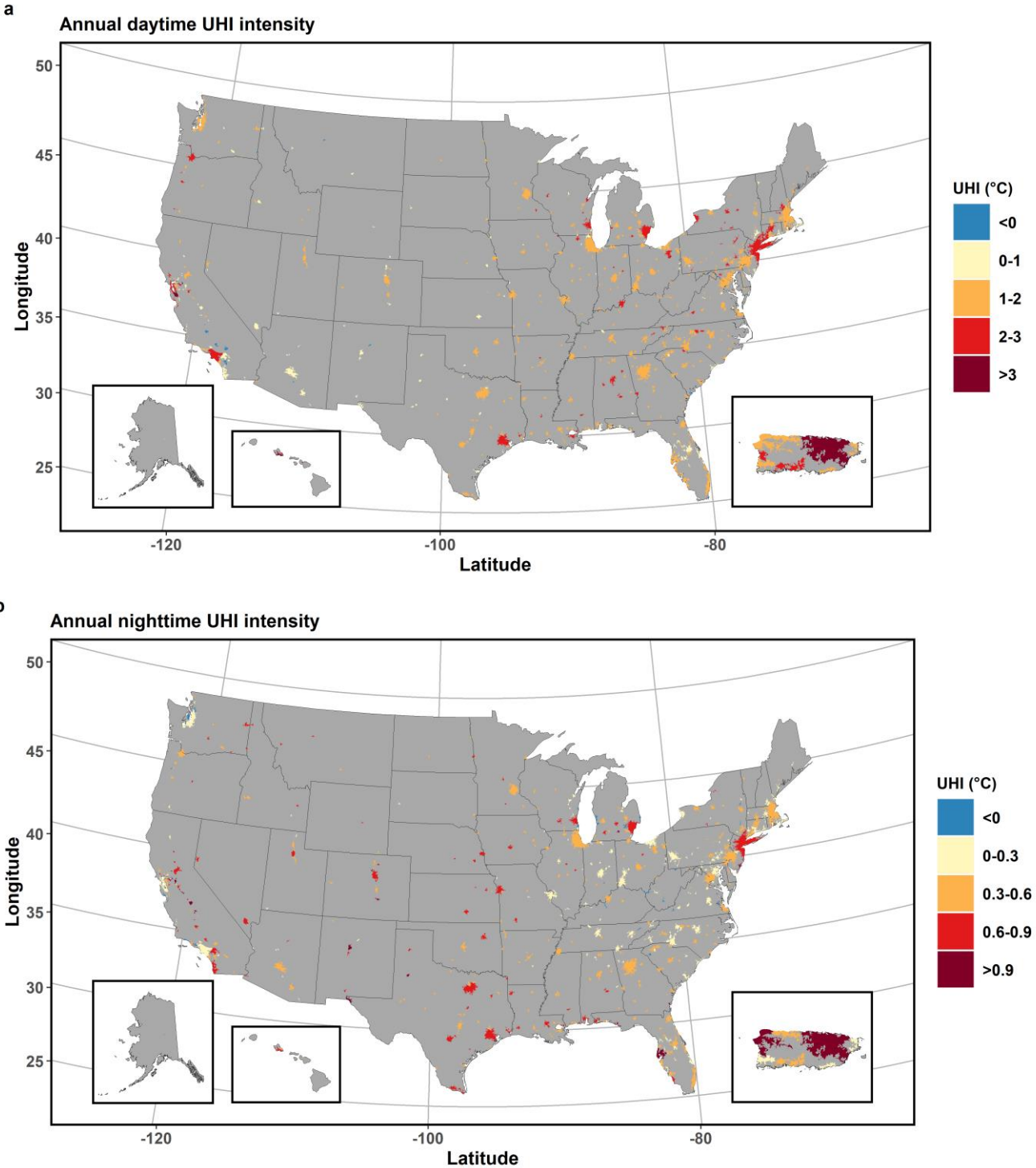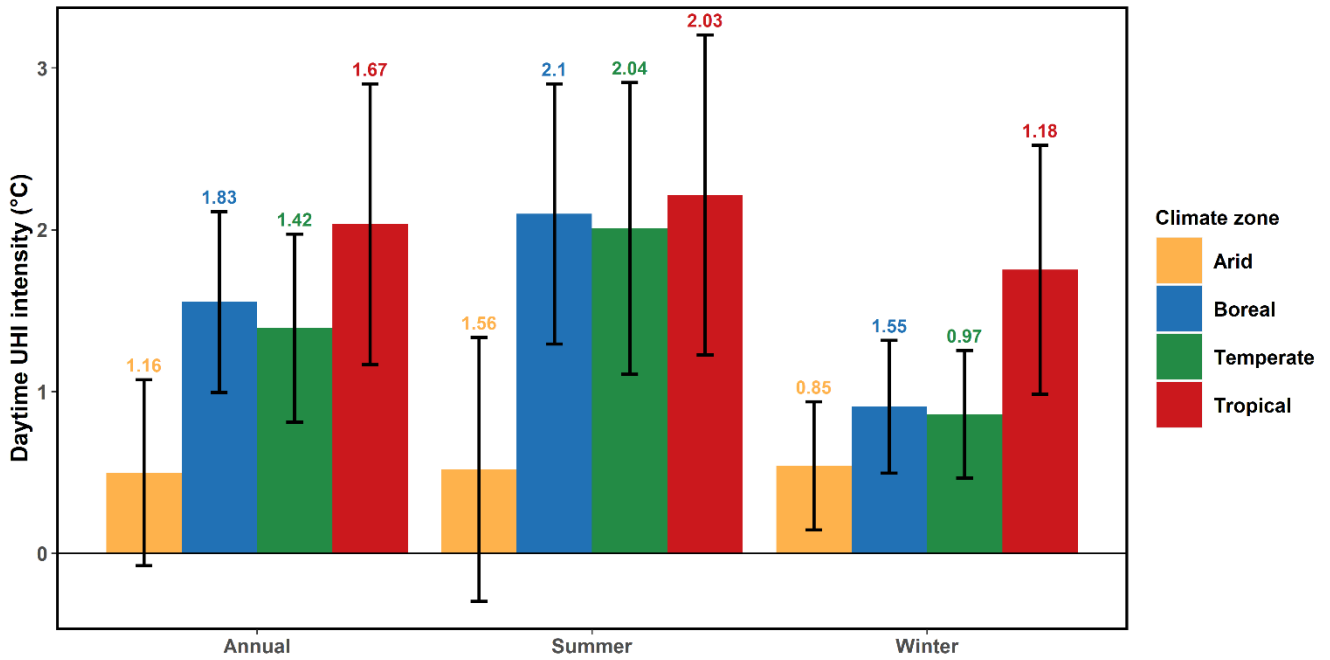
Fig. 2 Map of all urbanized areas in the US, along with their mean **(a)** annual daytime and **(b)** annual nighttime surface UHI intensity for 2013-2017. The sub-panels include Alaska, Hawaii, and Puerto Rico.
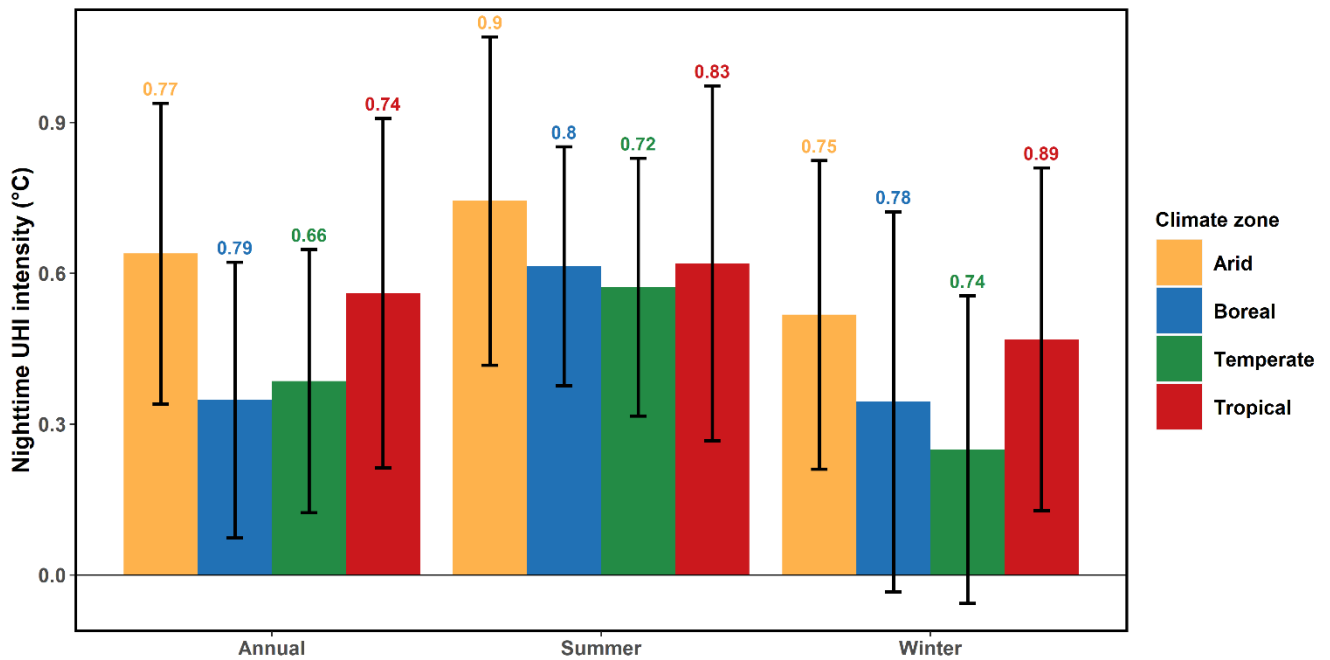
a

b

Fig. 3 Bar charts showing 2013-2017 mean annual, summertime, and wintertime daytime **(a)** and nighttime **(b)** surface UHI intensity of the urbanized areas for each climate zone. The error bars represent the standard deviation of the mean urban daytime surface UHI for each case, while the number at the top of the bars represent the pooled standard deviation of intra-urban daytime surface UHI intensity for the respective cases.

Table 1 Summary of calculated surface UHI intensities (mean ± standard deviation) for the cases considered in the present study. These values are not weighted by area.

Surface UHI	Case	Regions of interest				
		All US	Arid	Boreal	Temperate	Tropical
Annual daytime (°C)	All	1.38 ± 0.66	0.5 ± 0.57	1.55 ± 0.56	1.39 ± 0.58	2.03 ± 0.87
	Coastal	1.46 ± 0.77	0.23 ± 0	1.25 ± 0.54	1.36 ± 0.68	2.1 ± 0.9
	Non-Coastal	1.36 ± 0.63	0.5 ± 0.58	1.56 ± 0.56	1.4 ± 0.55	1.58 ± 0.64
Annual nighttime (°C)	All	0.4 ± 0.28	0.64 ± 0.3	0.35 ± 0.27	0.39 ± 0.26	0.56 ± 0.35
	Coastal	0.42 ± 0.34	0.64 ± 0	0.1 ± 0.19	0.4 ± 0.33	0.59 ± 0.36
	Non-Coastal	0.4 ± 0.27	0.64 ± 0.3	0.35 ± 0.27	0.38 ± 0.24	0.35 ± 0.04
Summer daytime (°C)	All	1.91 ± 0.97	0.52 ± 0.82	2.1 ± 0.8	2.01 ± 0.9	2.22 ± 0.99
	Coastal	1.98 ± 0.99	-0.27 ± 0	1.95 ± 0.61	1.95 ± 0.97	2.29 ± 1.01
	Non-Coastal	1.89 ± 0.97	0.54 ± 0.82	2.1 ± 0.81	2.02 ± 0.88	1.69 ± 0.84
Summer nighttime (°C)	All	0.6 ± 0.27	0.74 ± 0.33	0.61 ± 0.24	0.57 ± 0.26	0.62 ± 0.35
	Coastal	0.53 ± 0.31	0.58 ± 0	0.28 ± 0.22	0.52 ± 0.3	0.65 ± 0.37
	Non-Coastal	0.62 ± 0.25	0.75 ± 0.33	0.62 ± 0.23	0.59 ± 0.24	0.39 ± 0.05
Winter daytime (°C)	All	0.87 ± 0.45	0.54 ± 0.4	0.9 ± 0.41	0.86 ± 0.39	1.75 ± 0.77
	Coastal	0.98 ± 0.67	0.74 ± 0	0.6 ± 0.43	0.84 ± 0.52	1.8 ± 0.8
	Non-Coastal	0.85 ± 0.39	0.54 ± 0.4	0.91 ± 0.41	0.87 ± 0.35	1.39 ± 0.5
Winter nighttime (°C)	All	0.31 ± 0.34	0.52 ± 0.31	0.34 ± 0.38	0.25 ± 0.31	0.47 ± 0.34
	Coastal	0.35 ± 0.4	0.7 ± 0	0.01 ± 0.27	0.33 ± 0.4	0.5 ± 0.35
	Non-Coastal	0.3 ± 0.33	0.51 ± 0.31	0.35 ± 0.38	0.22 ± 0.27	0.25 ± 0.05

Table 2 Evaluation of urban-area weighted surface UHI intensities (mean ± standard deviation) calculated in present study using the database from the Global Surface UHI Explorer (https://yceo.yale.edu/research/global-surface-uhi-explorer; Chakraborty and Lee, 2019)

| Case	Study	Surface UHI Intensity (area-weighted)
Annual daytime (°C)	Chakraborty and Lee, 2019	1.27 ± 0.66
	Present study	1.54 ± 0.58
Annual nighttime (°C)	Chakraborty and Lee, 2019	0.4 ± 0.26
	Present study	0.43 ± 0.24
Summer daytime (°C)	Chakraborty and Lee, 2019	1.8 ± 0.94
	Present study	2.22 ± 0.93
Summer nighttime (°C)	Chakraborty and Lee, 2019	0.67 ± 0.31
	Present study	0.67 ± 0.22
Winter daytime (°C)	Chakraborty and Lee, 2019	0.73 ± 0.43
	Present study	0.95 ± 0.41
Winter nighttime (°C)	Chakraborty and Lee, 2019	0.26 ± 0.26
	Present study	0.34 ± 0.33
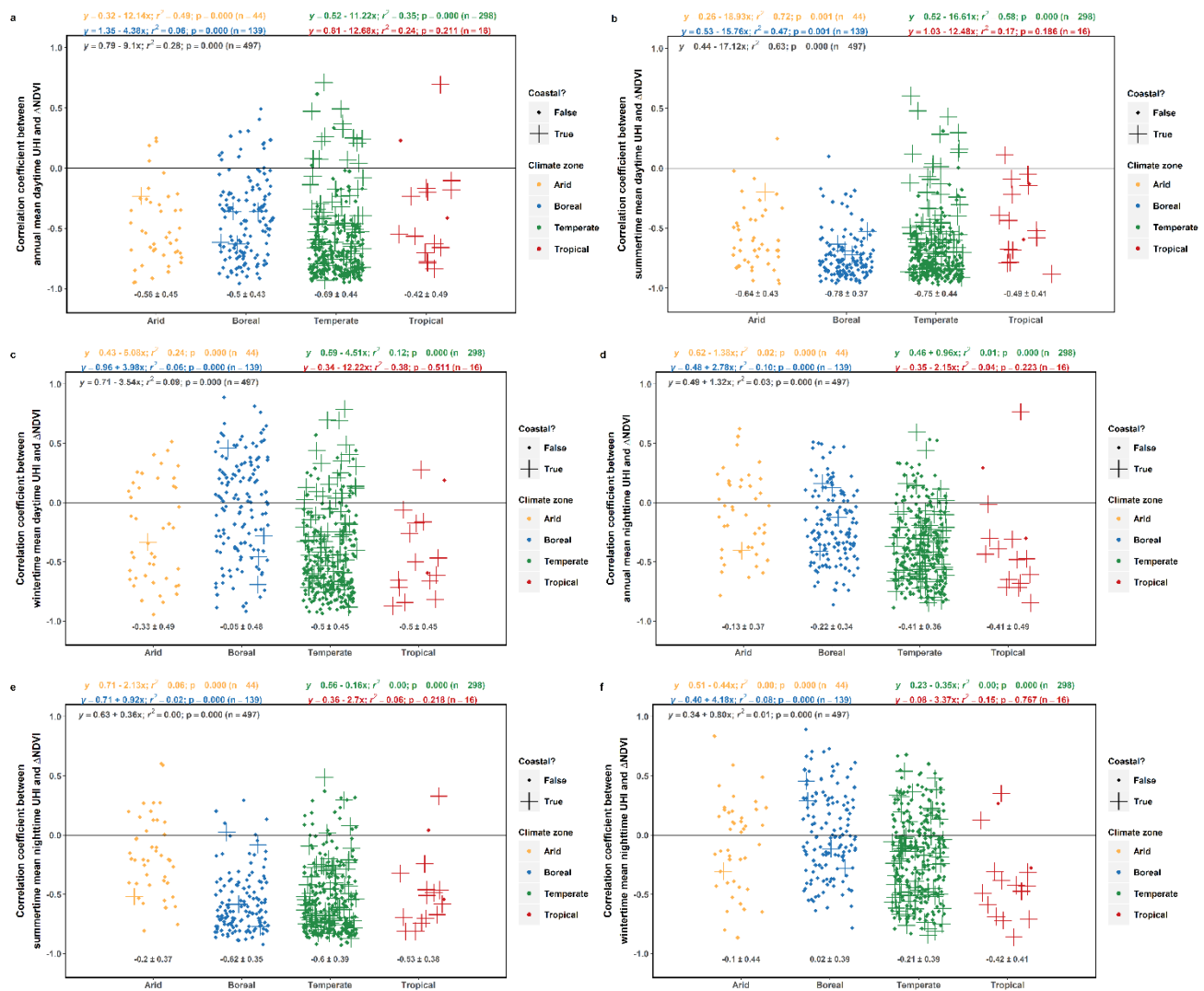
Fig. 4 Summary of intra-urban and inter-urban correlation between 2013-2017 **(a)** daytime surface UHI and mean annual ΔNDVI, **(b)** daytime surface UHI and mean summertime ΔNDVI, **(c)** daytime surface UHI and mean wintertime ΔNDVI**, (d)** nighttime surface UHI and mean annual ΔNDVI, **(e)** nighttime surface UHI and mean summertime ΔNDVI, and **(f)** nighttime surface UHI and mean wintertime ΔNDVI. The points show the distribution (jittered) of the Pearson correlation coefficient (r) between the two variables for every US urbanized area divided into the climate zones, calculated from the census tract-level calculations. The numbers below the points give the mean and standard deviation of r after Fisher's z transformation and back-transformation. The equations at the top show the correlations between the variables, calculated from the mean for each urbanized area (in black) and also sub-divided into the climate zones.
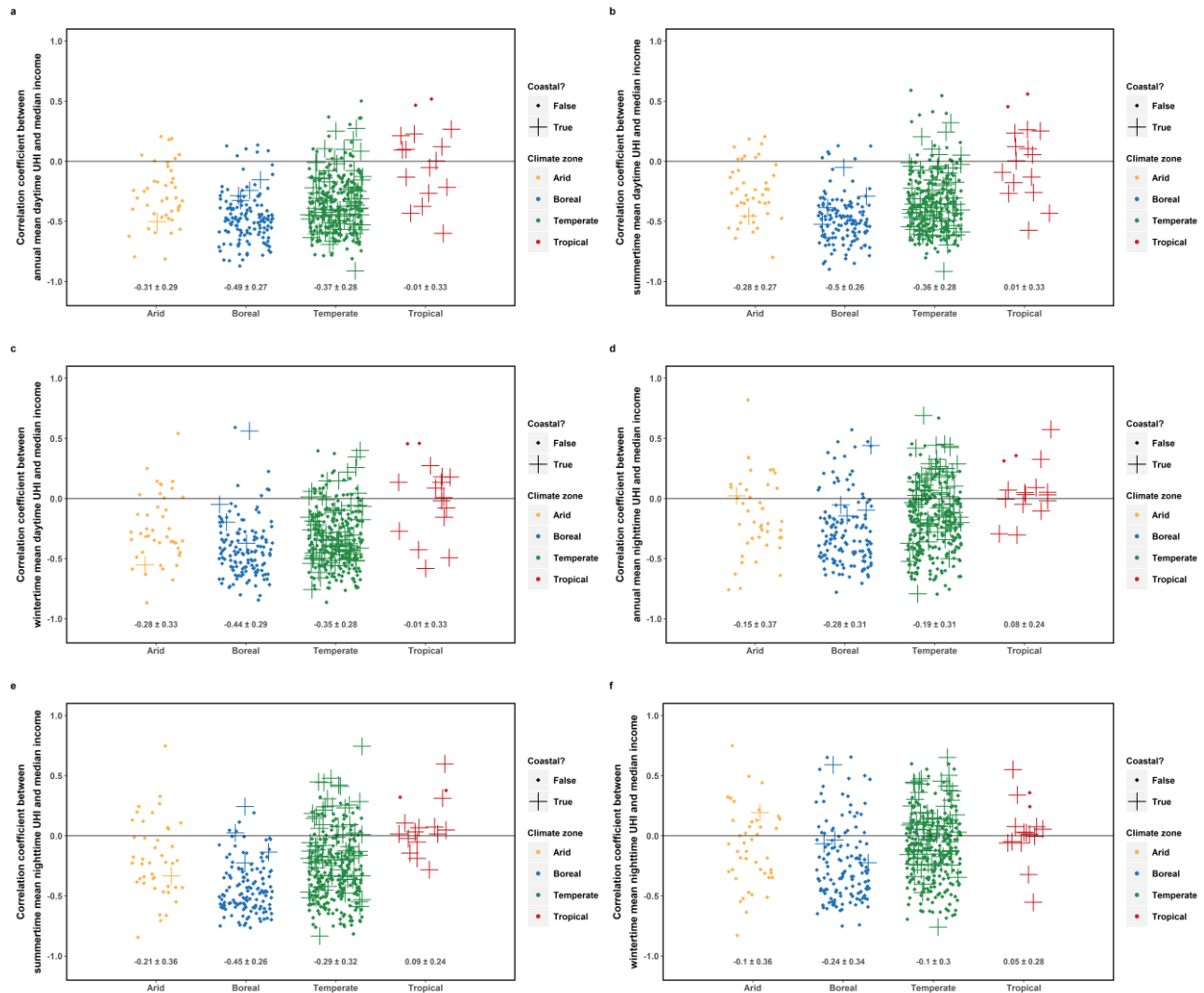
Fig. 5 Summary of intra-urban and inter-urban correlation of 2013-2017 **(a)** mean annual daytime surface UHI, **(b)** mean summertime daytime surface UHI, **(c)** mean wintertime daytime surface UHI, **(d)** mean annual nighttime surface UHI, **(e)** mean summertime nighttime surface UHI, and **(f)** mean wintertime nighttime surface UHI with 2017 median income. The points show the distribution (jittered) of the Pearson correlation coefficient (r) between the two variables for every US urbanized area divided into the climate zones, calculated from the census tract-level calculations. The numbers below the points give the mean and standard deviation of r after Fisher's z transformation and back-transformation.
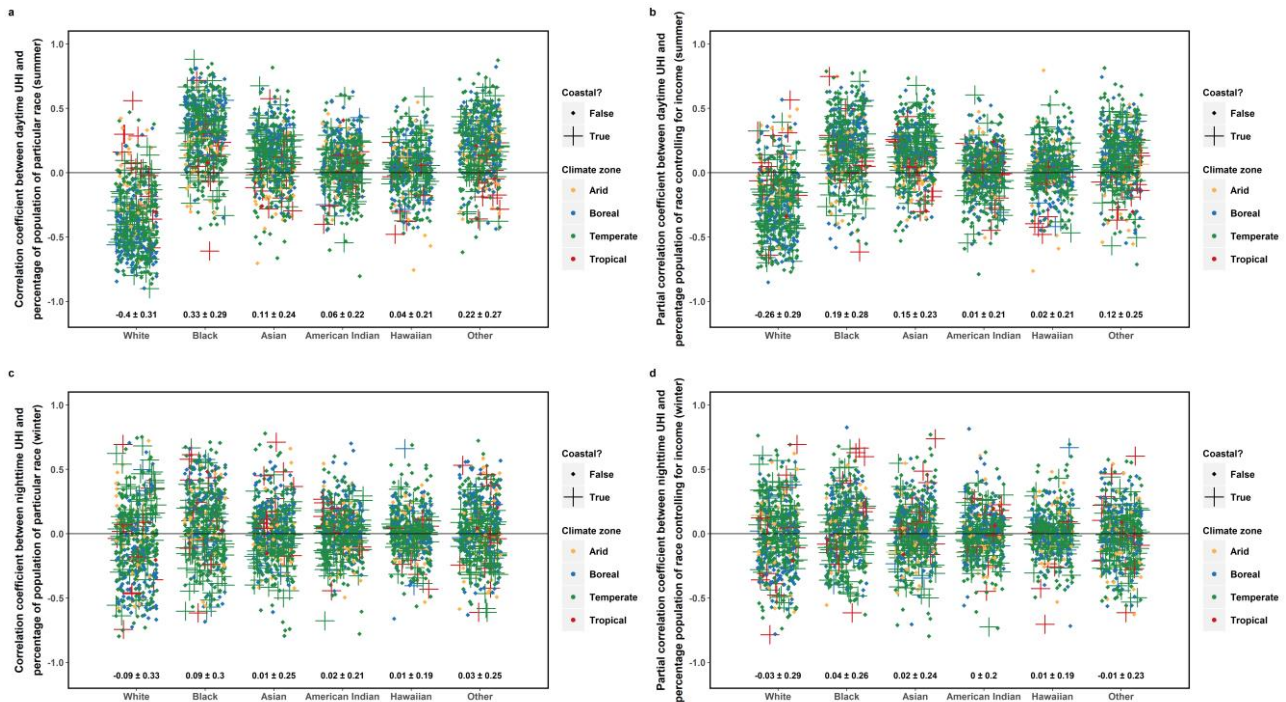
Fig. 6 Summary of intra-urban correlation of 2013-2017 mean **(a)** summertime daytime and **(c)** wintertime nighttime surface UHI with percentage of population belonging to each race. The points show the distribution (jittered) of the Pearson correlation coefficient (r) between the two variables for every US urbanized area divided into the climate zones, calculated from the census tract-level calculations. The numbers below the points give the mean and standard deviation of r after Fisher's z transformation and back-transformation. **(b)** and **(d)** Same as sub-figures **(a)** and **(c)**, but for the partial correlation coefficients after accounting for median income.
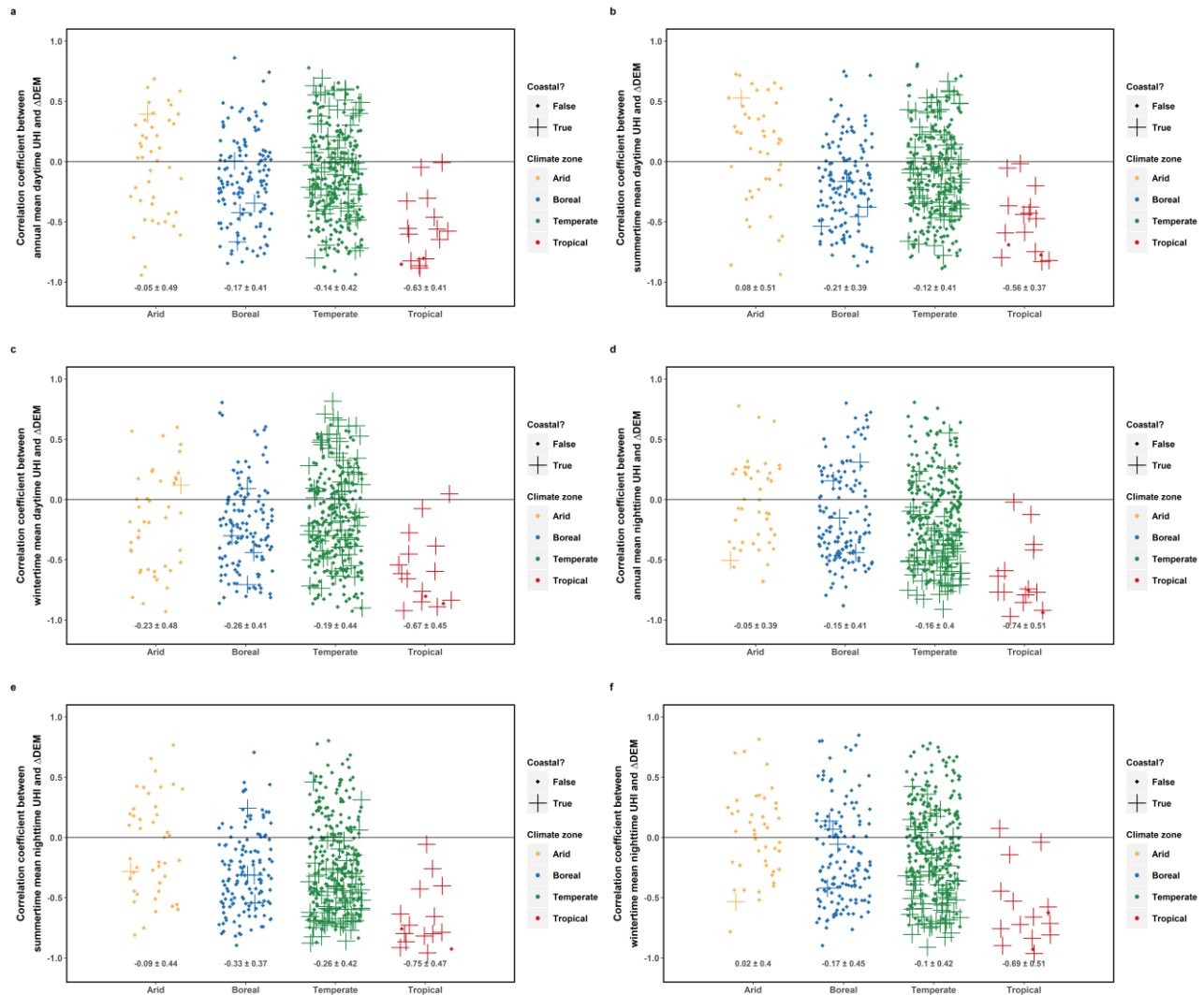
Fig. 7 Summary of intra-urban and inter-urban correlation of 2013-2017 **(a)** mean annual daytime surface UHI, **(b)** mean summertime daytime surface UHI, **(c)** mean wintertime daytime surface UHI, **(d)** mean annual nighttime surface UHI, **(e)** mean summertime nighttime surface UHI, and **(f)** mean wintertime nighttime surface UHI with ΔDEM. The points show the distribution (jittered) of the Pearson correlation coefficient (r) between the two variables for every US urbanized area divided into the climate zones, calculated from the census tract-level calculations. The numbers below the points give the mean and standard deviation of r after Fisher's z transformation and back-transformation.
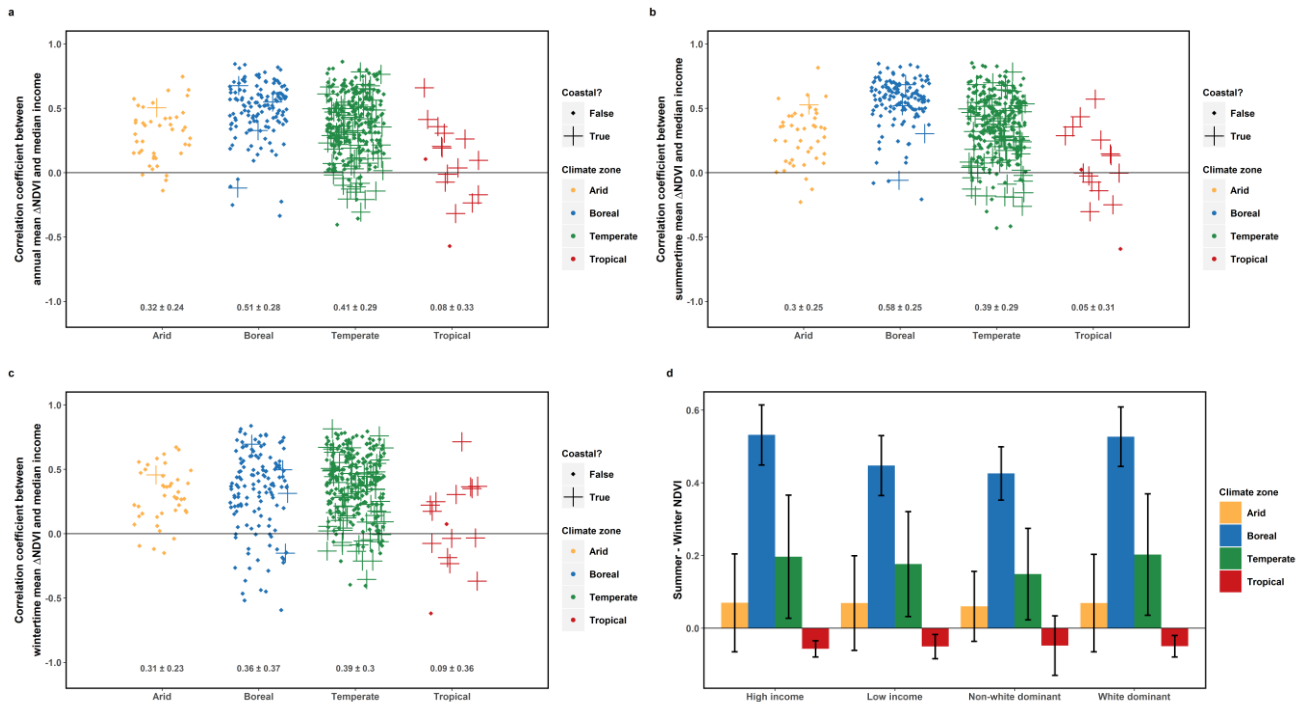
Fig. 8 Summary of intra-urban and inter-urban correlation of 2013-2017 **(a)** mean annual ΔNDVI, **(b)** mean summertime ΔNDVI, and **(c)** mean wintertime ΔNDVI with 2017 median income. The points show the distribution (jittered) of the Pearson correlation coefficient (r) between the two variables for every US urbanized area divided into the climate zones, calculated from the census tract-level calculations. The numbers below the points give the mean and standard deviation of r after Fisher's z transformation and back-transformation. **(d)** Difference between summertime and wintertime NDVI for high income (over 75 percentile for each urbanized area), low income (under 25 percentile for each urbanized area), white dominant (over 75% white), non-white dominant (under 25% white) census tracts. The bars represent the composite means from all urbanized areas grouped into the four climate classes while the error bars represent the standard deviation for each case.